星形成ゼミ

SF Newsletter 332
#1 ~ #8
担当:川邊
2020.09.25

SF news letter 332: #1 - #8

1. **Search for Alignment of Disk Orientations in Nearby Star-Forming Regions: Lupus, Taurus, Upper Scorpius, ρ Ophiuchi, and Orion**

   Masataka Aizawa[1,2], Yasushi Suto[1,3], Yoko Oya[1,3], Shiro Ikeda[4,5,6], and Takeshi Nakazato[6]

   [1] Department of Physics, The University of Tokyo, Tokyo 113-0033, Japan; [2] College of Science, Ibaraki University,

2. **Studying star-forming processes at core and clump scales: the case of the young stellar object G29.862−0.0044**

   M.B. Areal[1], S. Paron[1], C. Fariña[2,3], M.E. Ortega[1], M. Celis Peña[1], and M. Rubio[4]

3. **A Machine Learning model to infer planet masses from gaps observed in protoplanetary disks**

   Sayantan Auddy[1] and Min-Kai Lin[1]

4. **LEGO II: A 3 mm molecular line study covering 100 pc of one of the most actively star-forming portions within the Milky Way Disc**

   A.T. Barnes[1], J. Kauffmann[2], F. Bigiel[1], N. Brinkmann[3], D. Colombo[3], A.E Guzman[4], W.J. Kim[5], L.

5. **High Resolution Infrared Spectroscopy of Hot Molecular Gas in AFGL 2591 and AFGL 2136: Accretion in the Inner Regions of Disks Around Massive Young Stellar Objects**

   Andrew G. Barr[1], Adwin Boogert[2], Curtis N. DeWitt[3], Edward Montiel[3], Matthew J. Richter[4], John

6. **CMZoom: Survey Overview and First Data Release**

   Cara Battersby[1,2], Eric Keto[2], Daniel Walker[3,4], Ashley Barnes[5], Daniel Callanan[6,2], Adam Ginsburg[7],

7. **Birth of convective low-mass to high-mass second Larson cores**

   Asmita Bhandare[1], Rolf Kuiper[2,1], Thomas Henning[1], Christian Fendt[1], Mario Flock[1] and Gabriel-Dominique Marleau[2,3,1]

   [1] Max-Planck-Institut für Astronomie, Königstuhl 17, D-69117 Heidelberg, Germany; [2] Institut für Astronomie und

8. **FAUST I. The hot corino at the heart of the prototypical Class I protostar L1551 IRS5**

   E. Bianchi[1], C. J. Chandler[2], C. Ceccarelli[1], C. Codella[3,1], N. Sakai[4], A. Lopez-Sepulcre[1,5], L. T.

1. Search for Alignment of Disk Orientations in Nearby Star-Forming Regions: Lupus, Taurus, Upper Scorpius, ρ Ophiuchi, and Orion

Masataka Aizawa[1,2], Yasushi Suto[1,3], Yoko Oya[1,3], Shiro Ikeda[4,5,6], and Takeshi Nakazato[6]

[1] Department of Physics, The University of Tokyo, Tokyo 113-0033, Japan; [2] College of Science, Ibaraki University,

Spatial correlations among proto-planetary disk orientations carry unique information on physics of multiple star formation processes. We select five nearby star-forming regions that comprise a number of proto-planetary disks with spatially-resolved images with ALMA and HST, and search for the mutual alignment of the disk axes. Specifically, we apply the Kuiper test to examine the statistical uniformity of the position angle (PA: the angle of the major axis of the projected disk ellipse measured counter-clockwise from the north) distribution. The disks located in the star-forming regions, except the Lupus clouds, do not show any signature of the alignment, supporting the random orientation. Rotational axes of 16 disks with spectroscopic measurement of PA in the Lupus III cloud, a sub-region of the Lupus field, however, exhibit a weak and possible departure from the random distribution at a 2σ level, and the inclination angles of the 16 disks are not uniform as well. Furthermore, the mean direction of the disk PAs in the Lupus III cloud is parallel to the direction of its filament structure, and approximately perpendicular to the magnetic field direction. We also confirm the robustness of the estimated PAs in the Lupus clouds by comparing the different observations and estimators based on three different methods including sparse modeling. The absence of the significant alignment of the disk orientation is consistent with the turbulent origin of the disk angular momentum. Further observations are required to confirm/falsify the possible disk alignment in the Lupus III cloud.

[背景]

- 星spin、disk回転、それらの整列・不整列は星形成プロセス・物理と関係する大事な情報
- 星団形成の母体となる分子雲の回転が有意に大きいと、スピン等の整列が起こると予想される。
- 乱流、磁場などの効果を考えると,シミュレーション等ではより複雑化。観測的な実証が必要

[研究目的・手法]

- 塵円盤のALMA+/HST images から円盤のPAを求めることで、整列の統計的な考察を行うこと (これまでの観測結果を利用)
- 統計的手法として“Kuiper test”: rotational invarianceに適応
- 領域は、Lupus, Taurus, Upper Sco, ρ-Oph, Orion
- Lupus 領域では、(ALMA) Sparse Modeling Imagesも独自利用

[結果と結論]

- Lupus-III 領域のみで、disk PAが、分子雲のfilament方向と整列している兆候を捉えた(Kuiper testで、~ 2σ)。
- 整列が見られないのは、角運動量の乱流起源説と整合的

Kuiper Test

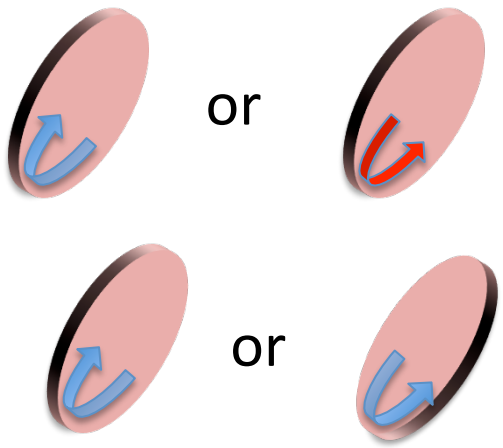

PA, inclinationの縮退あり

- gas kinematicsからPA縮退解ける=> Lupus
- inclinationの縮退は解けない

観測バイアス: i ≈ 0 (face-on) => 検出されやすい

- PAを用いて、”整列”の調査

Kuiper Test: 縮退のあるPAの統計に良く使われる

- uniform 分布のPA(累積)統計(F_{ref})と観測されたPA(累積) 統計(F_{obs})の違い(D)用いる(Dが大きいと、non-uniform)。

$$D = \max_{1 \leqslant n \leqslant N} [F_{\rm ref}(\mathrm{PA}_n) - F_{\rm obs}(\mathrm{PA}_n)] + \max_{1 \leqslant n \leqslant N} [F_{\rm obs}(\mathrm{PA}_n) - F_{\rm ref}(\mathrm{PA}_n)],$$

p-value, p_{null} (D)
$D>D_{obs}$を与えるprobability
p ~ 0.05 = > 2σ
p~ 0.003 => 3σ

0≤PA< 180 degの場合は、PAの平均、標準偏差の導出は、Marida & Jupp(2009)の手法に従う。

Five SF Regions & Summary

「観測データ]
Taurus: これまでの電波観測
(NMA, SMA, PdBI, CARMA ,ALMA)
ONC: HSTによる silhouette disks
(ALMAデータはavailableだが、
artificial effectで、6σのalignment
を検出。=> HST利用)
それ以外: ALMA

[距離]
ONC: ~400 pc
それ以外: 137-150 pc

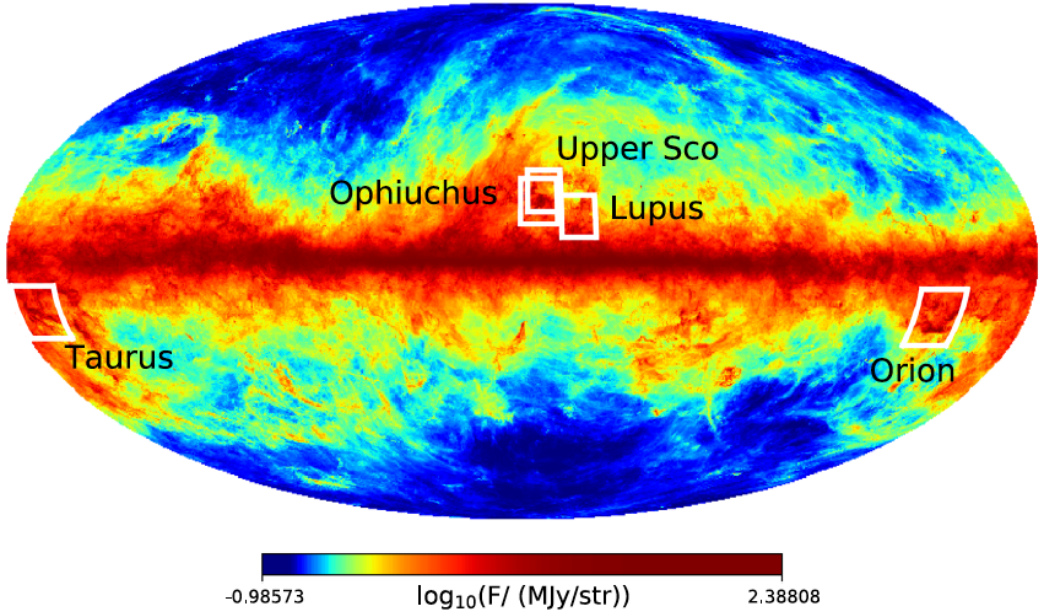

Figure 1. Map of the five star-forming regions analyzed in this paper overlaid on the thermal dust emission at 353 GHz (Planck Collaboratio

Table 1
Summary of Star-forming Regions along with Analyses of Alignment

Field	# Disk	Field Size/Resolution	Wavelength	p (Kuiper's Test)	Mean(PA) $\pm$ σ(PA)	Reference
Lupus	37	$7^\circ/0\farcs3$	Radio/ALMA	0.29	$31\farcs8 \pm 114\farcs4$[a]	(1)
- Lupus III	16/37	$0\farcs5/0\farcs3$	Radio/ALMA	0.037	$77\farcs3 \pm 69\farcs9$[a]	(1)
- Outside Lupus III cloud	21/37	$7^\circ/0\farcs3$	Radio/ALMA	0.30	$298\farcs6 \pm 94\farcs3$[a]	(1)
Taurus	50	$15^\circ/0\farcs4$–$1''$	Radio[b]	0.69	$178\farcs66 \pm 57\farcs4$	(2)–(7)
Upper Scorpius	16	$8^\circ/0\farcs37$	Radio/ALMA	0.16	$14\farcs6 \pm 39\farcs9$	(8)
Ophiuchus	49	$3^\circ/0\farcs2$	Radio/ALMA	0.68	$165\farcs5 \pm 59\farcs1$	(9), (10)
- L1688	31/49	$0\farcs5/0\farcs2$	Radio/ALMA	0.95	$156\farcs4 \pm 59\farcs4$	(9), (10)
ONC	31	$6'/0\farcs1$	Optical/HST	0.47	$21\farcs3 \pm 55\farcs9$	(11)

Lupusの結果:0 ≤ PA < 360

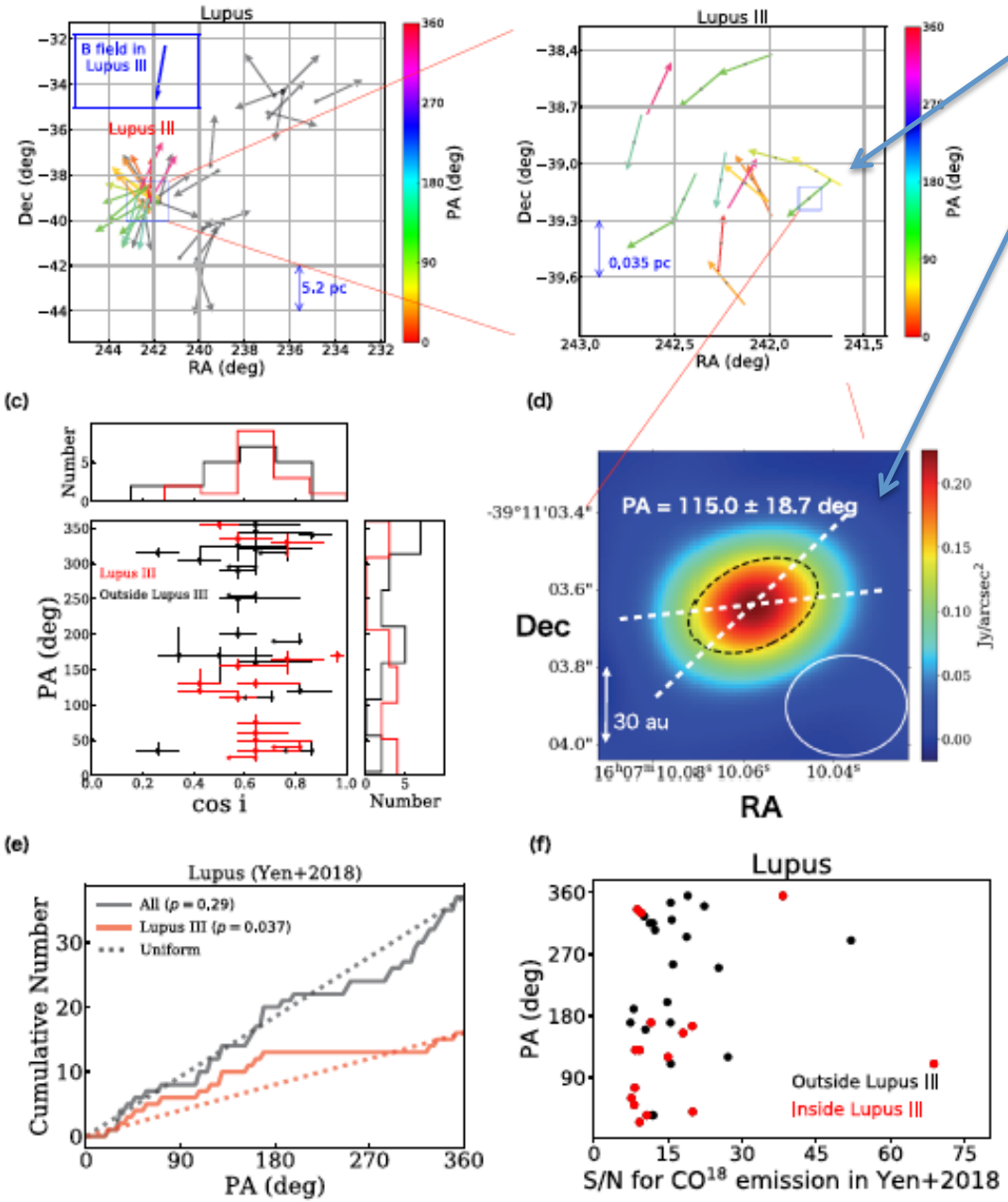

矢印はPA(major axis) 方向

黒破線: beam-deconvolved size

様々な方法で導出したPA

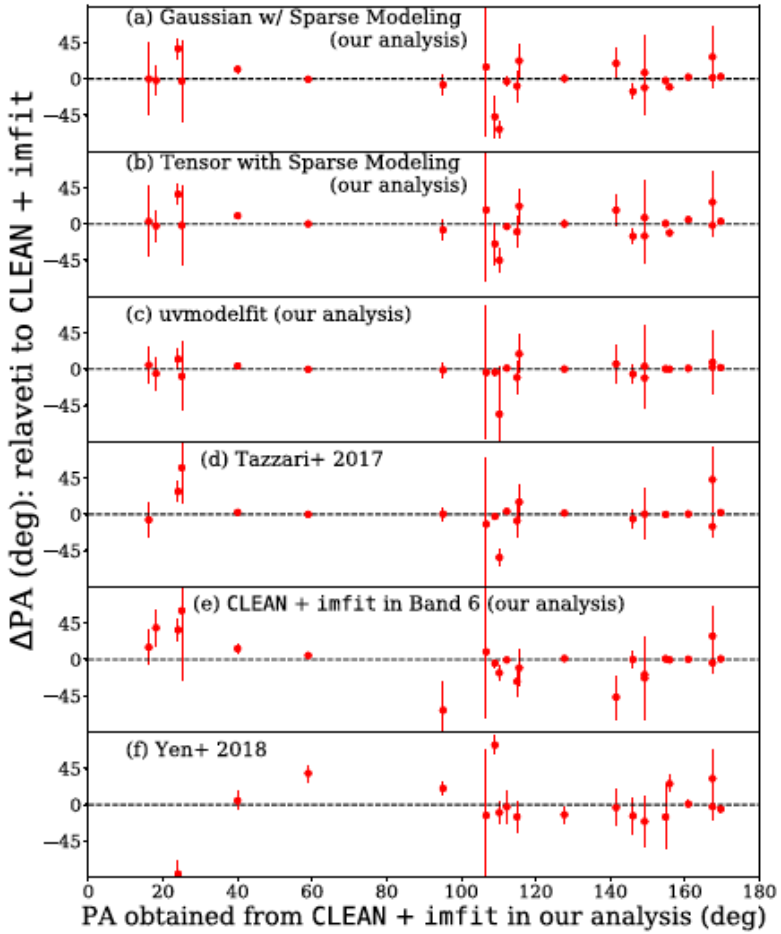

その他の領域:
Taurus, Upper Sco, Oph, ONC

いずれもAlignment未検出

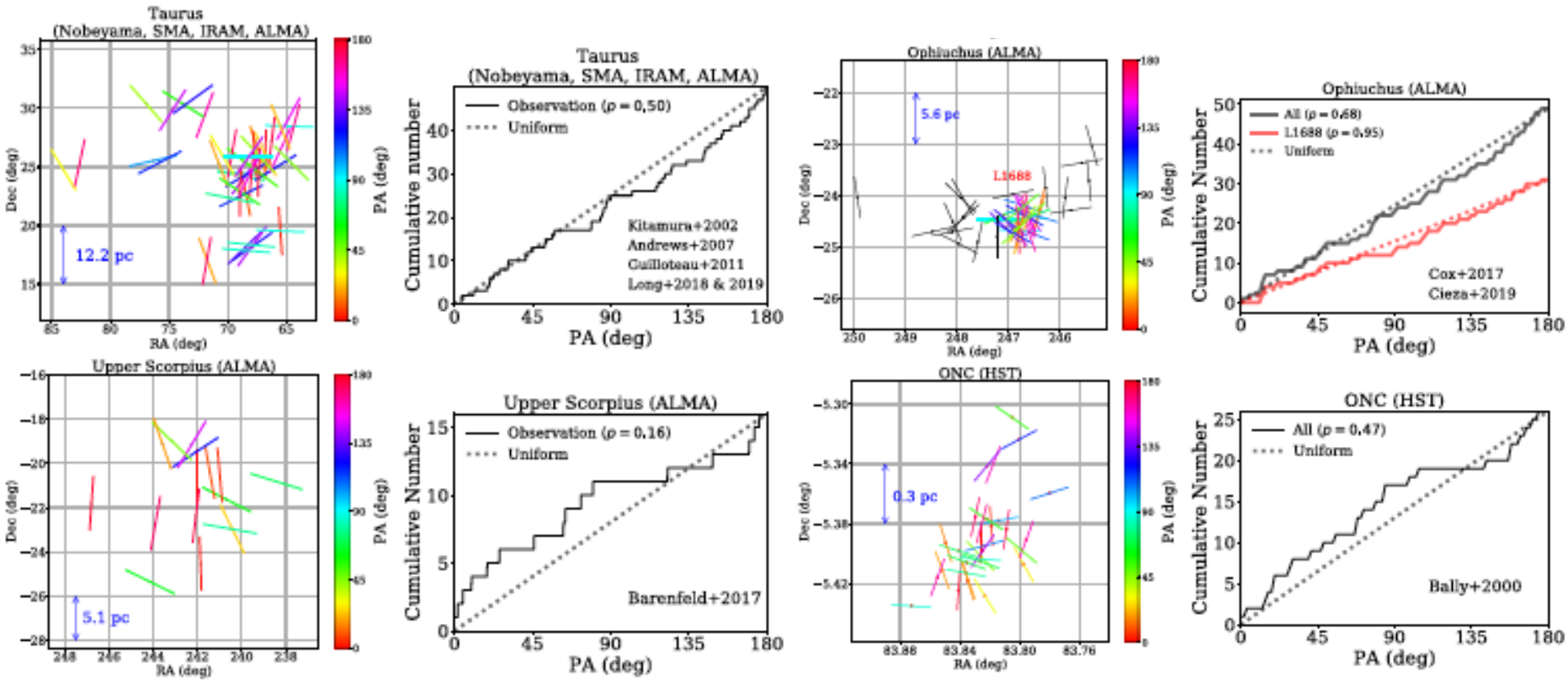

(補足:スパースモデリング)

Super-resolution Imaging of the Protoplanetary Disk HD 142527 Using Sparse Modeling

Masayuki Yamaguchi[1,2], Kazunori Akiyama[2,3,4,5,10], Takashi Tsukagoshi[2], Takayuki Muto[6], Akimasa Kataoka[2,7], Fumie Tazaki[2], Shiro Ikeda[8,9], Misato Fukagawa[1,2], Mareki Honma[1,2,7], and Ryohei Kawabe[1,2,7]
[1] Department of Astronomy, Graduate School of Science, The University of Tokyo, 7-3-1 Hongo, Bunkyo-ku, Tokyo 113-0033, Japan
masayuki.yamaguchi.astro@gmail.com

ApJ, 895, 84, 2020

スパースモデリング

- 画像(解)にスパース性を仮定することで、劣決定問題(未知数>測定数)を解決して、解を求める方法(圧縮センシングとも言われる)。非ゼロの解を制限してスパース解を求める。
- 2つの”罰則項”(regularization func.)を2つ導入する。L1-norm (非ゼロ絶対値の和)と TSV-norm (画像平坦度)
- 交差検証(cross varidation)で、最適解を求める
- 空間分解能は、CLEAN(通常の回折限界)の3-4倍を達成可能

$$\boldsymbol{I} = \underset{\boldsymbol{I}}{\operatorname{argmin}} \left(|\boldsymbol{W}(\boldsymbol{V} - \boldsymbol{F}\boldsymbol{I})|_2^2 + \Lambda_l \sum_i \sum_j |I_{i,j}| + \Lambda_t \sum_i \sum_j (|I_{i+1,j} - I_{i,j}|^2 + |I_{i,j+1} - I_{i,j}|^2) \right),$$

スパースモデリングの流れ

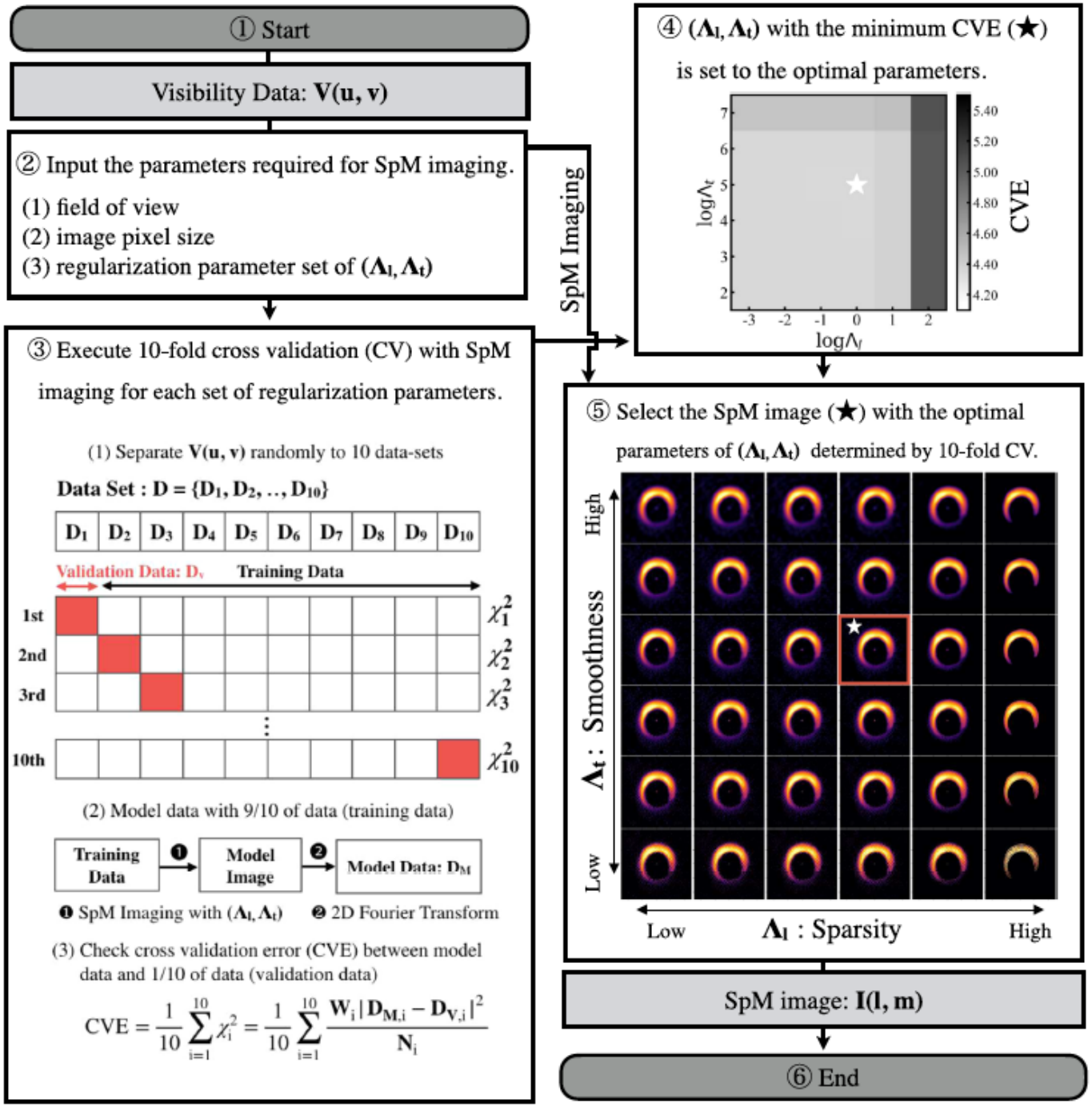

Yamaguchi+2020

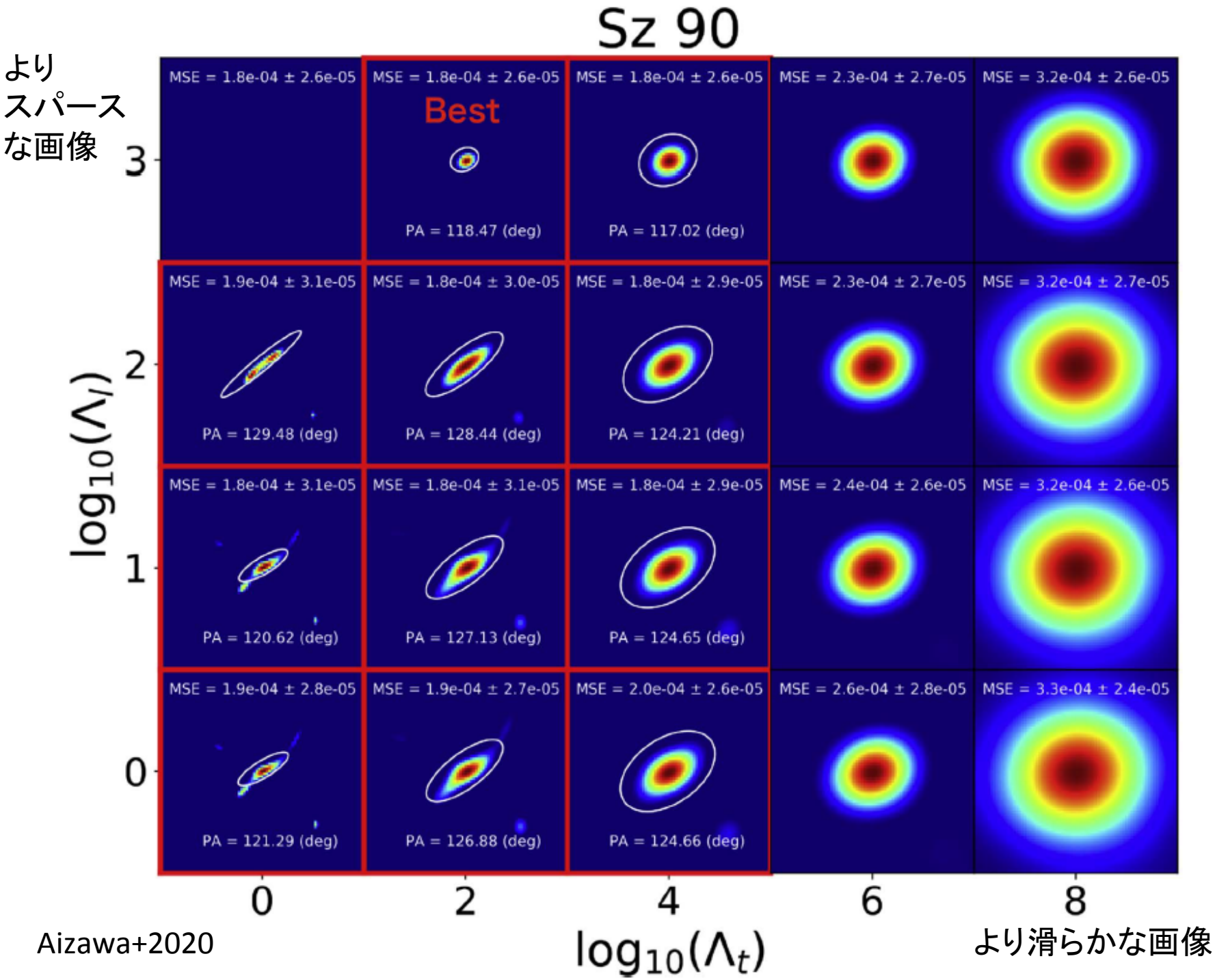
Sz 90
より
スパース
な画像
MSE = 1.8e-04 ± 2.6e-05
MSE = 1.8e-04 ± 2.6e-05
Best
MSE = 1.8e-04 ± 2.6e-05
MSE = 2.3e-04 ± 2.7e-05
MSE = 3.2e-04 ± 2.6e-05
PA = 118.47 (deg)
PA = 117.02 (deg)
MSE = 1.9e-04 ± 3.1e-05
MSE = 1.8e-04 ± 3.0e-05
MSE = 1.8e-04 ± 2.9e-05
MSE = 2.3e-04 ± 2.7e-05
MSE = 3.2e-04 ± 2.7e-05
PA = 129.48 (deg)
PA = 128.44 (deg)
PA = 124.21 (deg)
MSE = 1.8e-04 ± 3.1e-05
MSE = 1.8e-04 ± 3.1e-05
MSE = 1.8e-04 ± 2.9e-05
MSE = 2.4e-04 ± 2.6e-05
MSE = 3.2e-04 ± 2.6e-05
PA = 120.62 (deg)
PA = 127.13 (deg)
PA = 124.65 (deg)
MSE = 1.9e-04 ± 2.8e-05
MSE = 1.9e-04 ± 2.7e-05
MSE = 2.0e-04 ± 2.6e-05
MSE = 2.6e-04 ± 2.8e-05
MSE = 3.3e-04 ± 2.4e-05
PA = 121.29 (deg)
PA = 126.88 (deg)
PA = 124.66 (deg)
3
2
1
0
$\log_{10}(\Lambda_l)$
0
2
4
6
8
$\log_{10}(\Lambda_t)$
より滑らかな画像

Aizawa+2020

7. Birth of convective low-mass to high-mass second Larson cores

Asmita Bhandare[1], Rolf Kuiper[2,1], Thomas Henning[1], Christian Fendt[1], Mario Flock[1] and Gabriel-Dominique Marleau[2,3,1]

[1] Max-Planck-Institut für Astronomie, Königstuhl 17, D-69117 Heidelberg, Germany; [2] Institut für Astronomie und

Stars form as an end product of the gravitational collapse of cold, dense gas in magnetized molecular clouds. This fundamentally multi-scale scenario occurs via the formation of two quasi-hydrostatic Larson cores and involves complex physical processes, which require a robust, self-consistent numerical treatment. The primary aim of this study is to understand the formation and evolution of the second hydrostatic Larson core and the dependence of its properties on the initial cloud core mass. We used the PLUTO code to perform high-resolution, one- and two-dimensional radiation hydrodynamic (RHD) core collapse simulations. We include self-gravity and use a grey flux-limited diffusion approximation for the radiative transfer. Additionally, we use for the gas equation of state density- and temperature-dependent thermodynamic quantities (heat capacity, mean molecular weight, etc.) to account for effects such as dissociation of molecular hydrogen, ionisation of atomic hydrogen and helium, and molecular vibrations and rotations. Properties of the second core are investigated using one-dimensional studies spanning a wide range of initial cloud core masses from 0.5 $M_\odot$ to 100 $M_\odot$. Furthermore, we expand to two-dimensional (2D) collapse simulations for a selected few cases of 1 $M_\odot$, 5 $M_\odot$, 10 $M_\odot$, and 20 $M_\odot$. We follow the evolution of the second core for $\geq$ 100 years after its formation, for each of these non-rotating cases. Our results indicate a dependence of several second core properties on the initial cloud core mass. Molecular cloud cores with a higher initial mass collapse faster to form bigger and more massive second cores. The high-mass second cores can accrete at a much faster rate of $\approx 10^{-2} M_\odot\ yr^{-1}$ compared to the low-mass second cores, which have accretion rates as low as $10^{-5} M_\odot\ yr^{-1}$. For the first time, owing to a resolution that has not been achieved before, our 2D non-rotating collapse studies indicate that convection is generated in the outer layers of the second core, which is formed due to the gravitational collapse of a 1 $M_\odot$ cloud core. Additionally, we find large-scale oscillations of the second accretion shock front triggered by the standing accretion shock instability (SASI), which has not been seen before in early evolutionary stages of stars. We predict that the physics within the second core would not be significantly influenced by the effects of magnetic fields or an initial cloud rotation. In our 2D RHD simulations, we find convection being driven from the accretion shock towards the interior of the second Larson core. This supports an interesting possibility that dynamo-driven magnetic fields may be generated during the very early phases of low-mass star formation.

[背景]

- 第二静水圧平衡ラーソンコア(以降、SC)の形成、進化、その物理過程を知ることは、星形成の基礎過程の理解にとって重要：複雑な物理過程が関係しており、ロバストで首尾一貫した数値計算が求められる。

[研究目的・手法]

- SCの形成・進化、初期コアの質量とコアの性質との関係を理解すること
- 高解像で、1次元+2次元の輻射流体コア収縮計算を実施(PLUTE codeを利用)
- 重力+greybody, flux-limited diffusion近似の輻射輸送
- 1次元計算: 初期分子雲コア質量を0.5 -100 太陽質量と広い範囲で計算
- 2次元計算: 1, 5, 10, 20 太陽質量コアに限定して計算

[結果と考察]

- 初期条件に依存した種々の性質を第二コアが持つこと：より大質量初期コアは、より早く収縮し、サイズ的に大きく、重い第二コアを形成
- 2Dの無回転コア収縮計算で、SC外層部に対流層ができることを発見
- SC衝撃波面での大規模な振動を見出した(降着衝撃波不安定性起源)。
- SC内の物理は、磁場や分子雲コアの回転に影響を受けないと予想される。

[結論]

- 降着流衝撃波に駆動された対流を見出した。この結果は、低質量星のごく初期で、ダイナモ駆動磁場が生み出される可能性を示唆している。

Numerical Method

Initial Setup

- stable BE sphere-like density profile

1D Setup: 0.5-100 M_{sun}、10^{-4} – 3000 au

2D setup

- Eulerian grid (axial & mid-plane symmetry)
- 1445 log-spaced cells
- 10^{-2} – 3000 au
- polar(0-90deg.): 180 cells

Boundary conditions (BD)

- reflective BD at inner edge (流体計算) & no 輻射flux
- "Dirichlet" BD at outer edge (constant radiation temperature)
- 2D: axisymmetric BDs at the pole and mirror-symmetric BDs at the equator

$$\rho_0 = \left(\frac{1.18\, c_{s0}^3}{M_0\, G^{3/2}}\right)^2 \qquad c_{s0}^2 = \frac{G M_0}{\ln(14.1)\, R_{\rm cloud}}.$$

$$\rho_c = 14.1\, \rho_0,$$

Table 1. Initial cloud core properties.

M_0 ($M_\odot$)	$R_{\rm cloud}$ (au)	T_0 (K)	$T_{\rm BE}$ (K)	$M_{\rm BE}/M_0$	ρ_c (g cm^{-3})
0.5	3000	10.0	9.49	1.05e−00	1.16e−17
1.0	3000	10.0	18.98	5.27e−01	2.33e−17
2.0	3000	10.0	37.96	2.64e−01	4.66e−17
5.0	3000	10.0	94.91	1.05e−01	1.17e−16
8.0	3000	10.0	151.85	6.58e−02	1.87e−16
10.0	3000	10.0	189.81	5.27e−02	2.33e−16
12.0	3000	10.0	227.78	4.39e−02	2.80e−16
14.0	3000	10.0	265.74	3.76e−02	3.26e−16
15.0	3000	10.0	284.72	3.51e−02	3.50e−16
16.0	3000	10.0	303.70	3.29e−02	3.73e−-16
18.0	3000	10.0	341.66	2.93e−02	4.20e−16
20.0	3000	10.0	379.63	2.63e−02	4.66e−16
30.0	3000	10.0	569.44	1.76e−02	6.99e−16
40.0	3000	10.0	759.25	1.32e−02	9.33e−16
60.0	3000	10.0	1138.88	8.78e−03	1.40e−15
80.0	3000	10.0	1518.50	6.58e−03	1.87e−15
100.0	3000	10.0	1898.13	5.27e−03	2.33e−15

Notes. List of the cloud core properties for runs with different initial cloud core mass M_0 ($M_\odot$), outer radius $R_{\rm cloud}$ (au), temperature T_0 (K), temperature $T_{\rm BE}$ (K) of a stable Bonnor–Ebert cloud core, stability parameter $M_{\rm BE}/M_0$, and central density ρ_c (g cm^{-3}).

1D Results

Second Coreは膨張を続けるが、
Kelvin Helmholtz 時間と降着時間が
一致すると膨張が止まり、収縮し始める

$$t_{\rm KH} = \frac{GM_{\rm sc}^2}{L_{\rm sc}\,R_{\rm sc}} \text{ and } t_{\rm accretion} = \frac{M_{\rm sc}}{\dot{M}_{\rm sc}},$$

Properties of the second core estimated at the final simulation snapshot $t_{\rm final}$ when central density $\rho_{\rm c,final}$ reaches ≈0.5–0.8 initial cloud core masses M_0 with a fixed outer radius $R_{\rm cloud}$ = 3000 au and an initial temperature T_0 = 10 K.

M_0 ($M_\odot$)	$\rho_{\rm c,final}$ (g cm^{-3})	$t_{\rm final}$ (yr)	$R_{\rm sc}$ (au)	$M_{\rm sc}$ ($M_\odot$)	$T_{\rm sc}$ (K)	$\dot{M}_{\rm sc}$ ($M_\odot$ yr^{-1})	$L_{\rm acc}$ ($L_\odot$)
0.5	0.854	38039.76	0.203	3.36e−02	2.07e+03	3.23e−05	7.78e−01
1.0	0.851	18635.00	0.253	4.40e−02	1.79e+03	6.52e−05	1.65e+00
2.0	0.853	11543.76	0.329	6.58e−02	1.67e+03	1.52e−04	4.43e+00
5.0	0.849	6860.80	0.405	1.65e−01	1.54e+03	5.53e−04	3.27e+01
8.0	0.848	5433.00	0.613	3.62e−01	1.50e+03	1.18e−03	1.01e+02
10.0	0.853	4909.00	0.876	5.73e−01	1.56e+03	1.71e−03	1.64e+02
12.0	0.849	4530.70	0.987	8.31e−03	8.62e+03	2.32e−03	2.85e+02
14.0	0.848	4251.80	1.290	1.17e+00	8.89e+03	3.01e−03	3.97e+02
15.0	0.835	4138.62	1.359	1.36e+00	8.77e+03	3.26e−03	4.77e+02
16.0	0.825	4015.29	1.455	1.50e+00	8.77e+03	3.61e−03	5.41e+02
18.0	0.792	3799.47	1.656	1.77e+00	8.77e+03	4.34e−03	6.75e+02
20.0	0.761	3610.66	1.914	2.01e+00	8.99e+03	5.17e−03	7.93e+02
30.0	0.662	2996.06	2.829	3.57e+00	8.97e+03	9.64e−03	1.77e+03
40.0	0.596	2623.36	3.803	5.25e+00	8.96e+03	1.50e−02	3.02e+03
60.0	0.519	2160.45	5.605	8.48e+00	1.04e+04	2.77e−02	6.11e+03
80.0	0.474	1859.02	5.486	1.08e+01	1.11e+04	4.20e−02	1.21e+04
100.0	0.448	1655.55	5.206	1.31e+01	1.16e+04	5.78e−02	2.12e+04

ıe properties listed are the second core radius $R_{\rm sc}$, mass $M_{\rm sc}$, temperature $T_{\rm sc}$, accretion rate $\dot{M}_{\rm sc}$, and accretion luminosity $L_{\rm ac}$

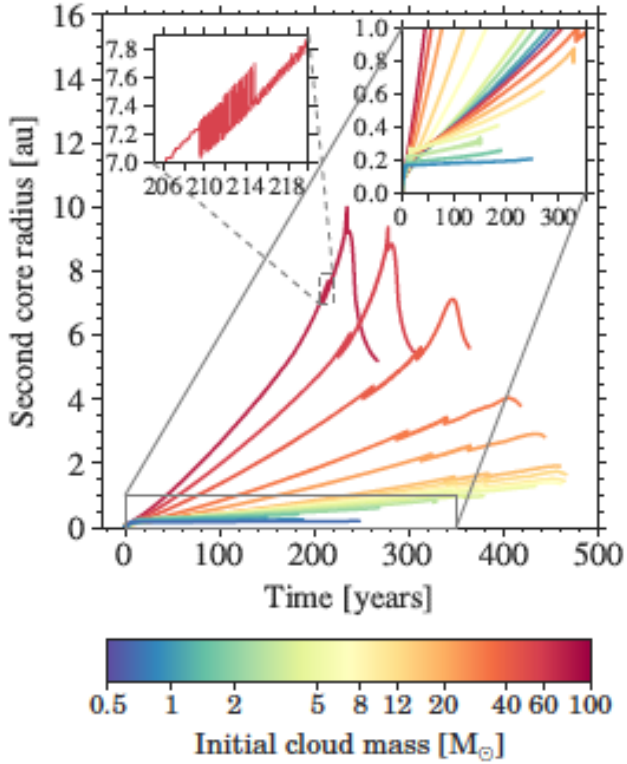

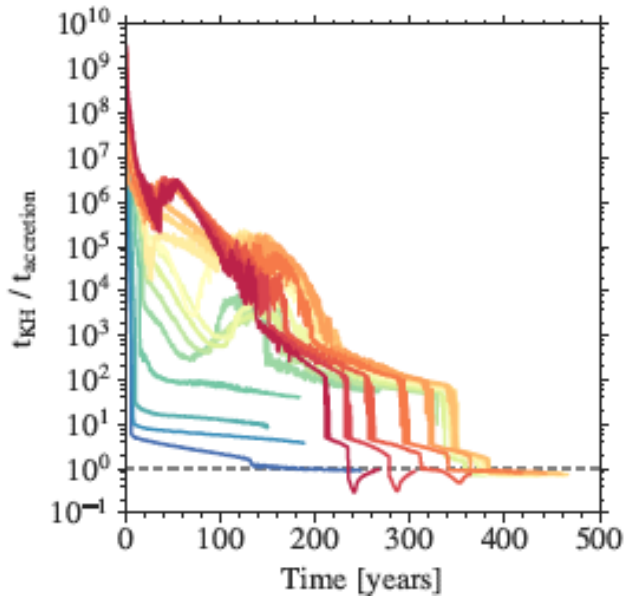

2D Results

1 Msun case:　t=312 yrs
衝撃波面の内側で
対流層が形成

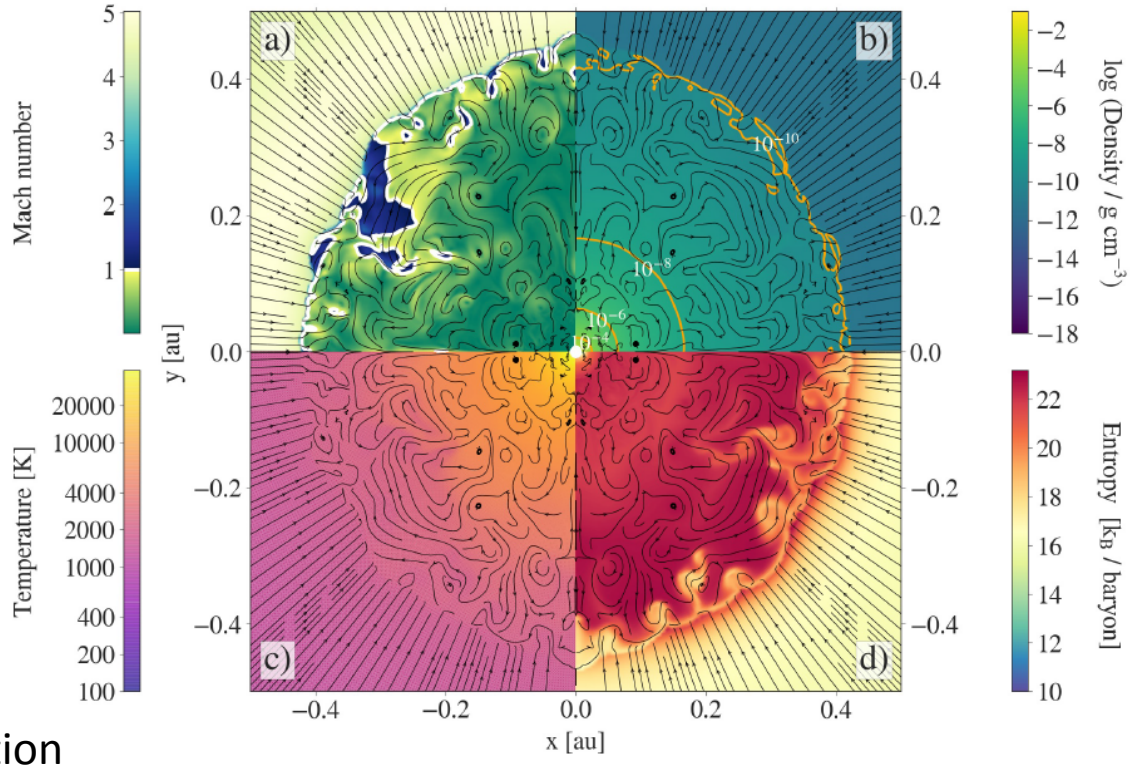

Line Integral Convolution Visualization

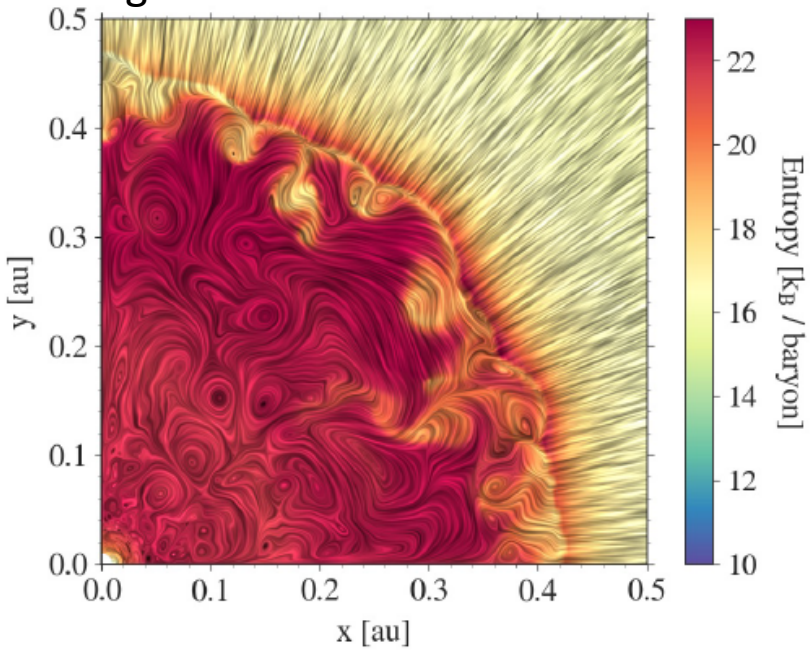

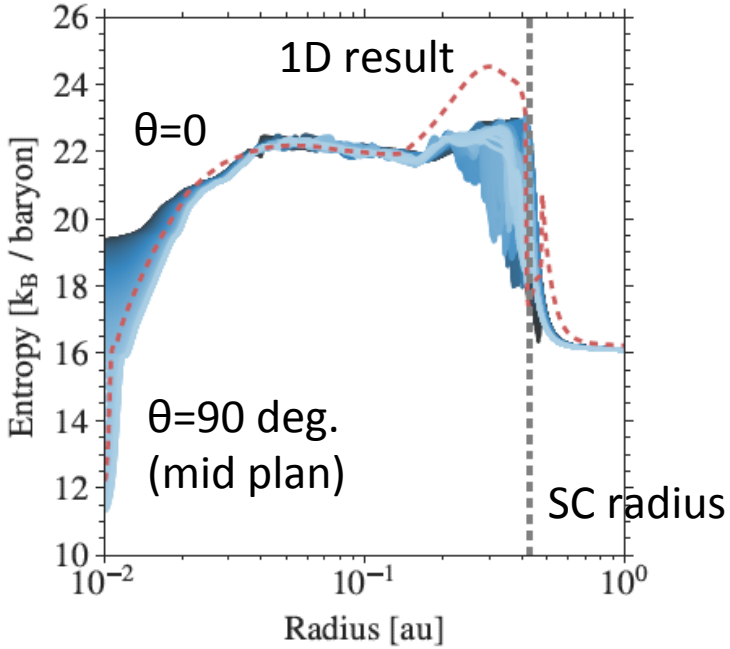

Standing Accretion Shock Instability(SASI)

Second Coreの表面が振動
(High Mass Coreは、比較的小さい)

SASIに寄る振動だが、超新星爆発のcore collapse時のSASIに比べると小規模

対流不安定性が、摂動の主な原因と考えられるが、SASIがAccretion Shockの振動に主に寄与している。

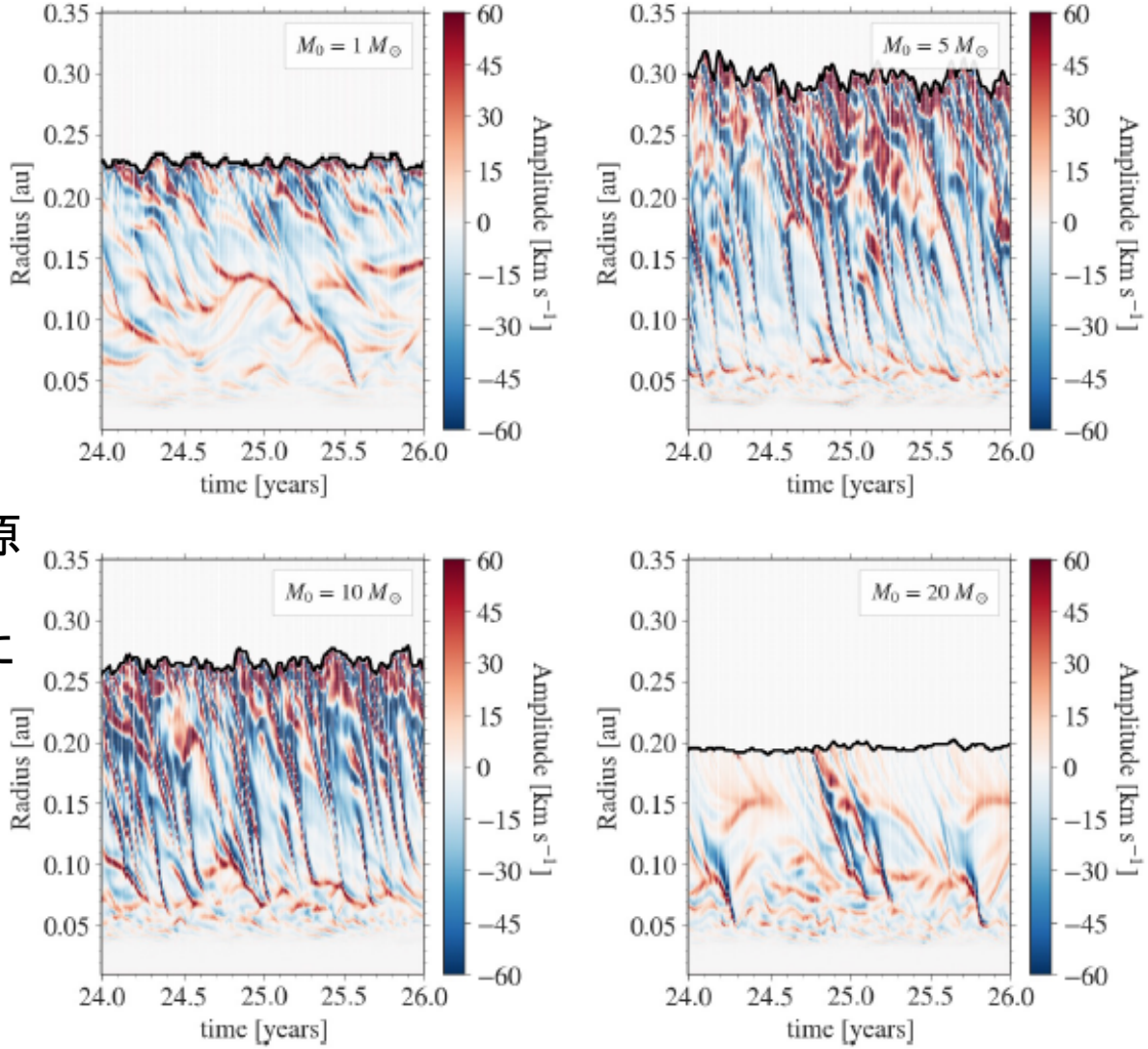

Fig. 14. Time evolution of the amplitude of the dominant spherical harmonics mode of the quantity $A(t, r, \theta)$ from Eq. (8). The second core radius is shown by the black line. The time $t = 0$ indicates the onset of the second core formation for the different collapse scenarios. Shown here is a small interval in time for the $1\,M_\odot$ (*top left*), $5\,M_\odot$ (*top right*), $10\,M_\odot$ (*bottom left*), and $20\,M_\odot$ (*bottom right*) cases.

Advected Perturbationの振幅変化

$$A(t, r, \theta) = \frac{1}{\sin\theta}\frac{\partial}{\partial\theta}(v_\theta(t, r, \theta)\sin\theta).$$

Comparison(1D, 1 M_{sun}) with previous work

<u>Msunaga & Inutsuka (2000)</u>: 1D & uniform cloud (1M_{sun})

- 4 R_{sun}/0.7 M_{sun} SC at a few x 10^3 yr (小さく重い)

<u>Tomida+(2013)</u>: 3D RMHD & BE-like cloud(1M_{sun})

- 10 R_{sun}/2 10^{-2} M_{sun} SC at 0.7 yr, その後SCが膨張すること示唆 (main accretion phase):今回の結果と整合的

<u>Vaytet & Haugbølle (2017)</u>: 1D & similar setup

- some difference due to different gas EOS

<u>Schönke & Tscharunuter (2011)</u>: grid-based 2D RHD

- collapse of rotating cloud (1 M_{sun})をsimulation
- viscosity parameter $\beta=10^{-2}$, 10^{-3}=> a<3 au 重力不安定
- convection が発生していることを示唆

2D vs 1D (破線)
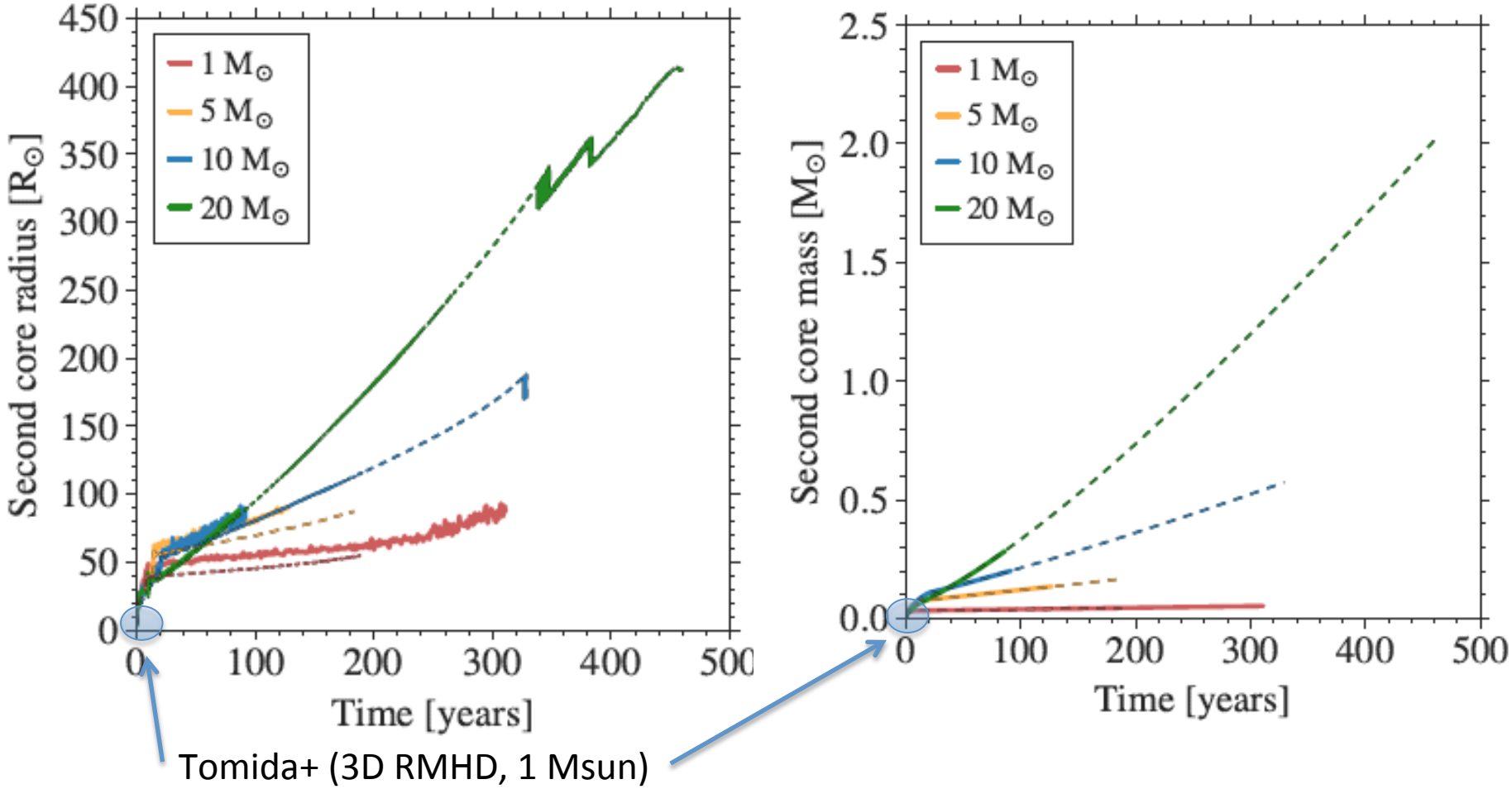
1D 計算は、2D の結果をほぼfollow
2Dの結果は、球対称からずれ=> 3D計算が必要(今は困難)
今後は、磁場、回転を含む1D/2D計算へ